J Mater Sci (2008) 43:6331–6336
DOI 10.1007/s10853-008-2922-5

Finite element analysis of deep indentation by a spherical indenter

Yuebin Charles Lu · Siva N. V. R. K. Kurapati · Fuqian Yang

Received: 9 May 2008 / Accepted: 31 July 2008 / Published online: 16 August 2008

Abstract Using the finite element analysis, the deep indentation of strain-hardening elastoplastic materials by a rigid, spherical indenter has been studied. The simulation results clearly show that the ratio of the indentation load to the maximum indentation depth increases with the increase of the strain-hardening index and reaches a maximum value at the maximum indentation depth being about 10% of the indenter radius. The power law relation between the indentation load and the indentation depth for shallow indentation becomes invalid for deep indentation. However, the ratio of the plastic energy to the total mechanical work is a linear function of the ratio of the residual indentation depth to the maximum indentation depth, independent of the strain-hardening index and the indentation depth.

Introduction

The indentation test is a technique for measuring mechanical properties of materials of small volume, including thin films and micromechanical structures. The test itself is based on the concept of the hardness test, in which both the resistance to penetration and the displacement of indenter are recorded and analyzed. Depending on the size of the indenter tip and the resolutions of the indentation depth and indentation load, indentations can be made on micron or nano level. As the technology of producing micromechanical and nanomechanical structures is going on increasing, the importance of characterizing mechanical properties at the submicron scale is going on increasing. This has stimulated the interest in understanding the indentation deformation of materials from continuum mechanics to molecular mechanics.

The indentation deformation consists of elastic and plastic deformation. Various methods have been developed in solving the indentation deformation of elastic materials [1–7], including the use of stress-potential functions and integral transforms. Analytical solutions have been obtained, which provide the rational of characterizing elastic properties of materials from the contact deformation. The elastoplastic deformation during indentation is much more complex, and there is no analytical solution describing the indentation deformation. Numerical analysis has become a major technique to study the indentation deformation of elastoplastic materials [8–15]. Shih et al. [8] evaluated the effect of the indenter tip on the relation between contact area and depth of indent. Montmitonnet et al. [9] performed the finite element analysis of spherical indentation on elastoplastic materials. They focused on the discussion of friction law and sliding/sticking threshold. Sadeghipour et al. [10] addressed the formation of ring cracks in the finite element analysis of spherical indentation of polymer-based materials. Shu and Fleck [11] analyzed a size effect in microindentation, using the theory of the strain gradient plasticity, and evaluated the effect of contact friction. Taljat et al. [12] used the finite element method to analyze spherical indentation of elastoplastic materials and established a procedure to construct stress–strain curves. Ni et al. [16] examined the spherical indentation of elastoplastic materials with work hardening and obtained two relations among mechanical properties and the indentation parameters. However, most studies focused on shallow

Y. C. Lu · S. N. V. R. K. Kurapati
Department of Mechanical Engineering, University of Kentucky, Lexington, USA

F. Yang (✉)
Department of Chemical and Materials Engineering, University of Kentucky, Lexington, KY 40506, USA
e-mail: fyang0@engr.uky.edu

indentation. There is little study on deep indentation of elastoplastic materials by a spherical indenter and on the dependence of the dissipated plastic energy on the strain-hardening index in an indentation loading–unloading cycle.

The purpose of this work is to use the finite element method to analyze the indentation of elastoplastic materials by a rigid, spherical indenter. The elastoplastic materials are modeled by a power-law constitutive relationship between stress and strain. In contrast to the work reported in literature, the focuses are on deep indentation and on the effect of the strain-hardening index on the indentation deformation. Discussions are also given on the effect of the strain-hardening index on the energy ratio of the dissipated plastic energy to the total mechanical work. In the simulation, we assume: (1) the material is isotropic and homogeneous, (2) the system is isothermal, and (3) the material is not subjected to body force.

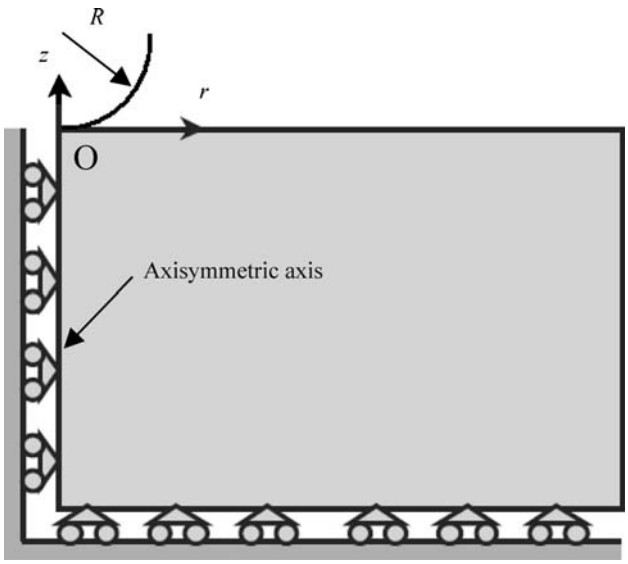

Fig. 1 Schematic of the axisymmetric indentation of a semi-infinite elastoplastic material

Boundary value problem

For an elastoplastic material obeying the power-law relation, the 1-D stress–strain relation subjected to uniaxial stress is

$$\sigma = \begin{cases} E\varepsilon & \text{for } \varepsilon \le \sigma_y/E \\ \sigma_y(E\varepsilon/\sigma_y)^n & \text{for } \varepsilon \ge \sigma_y/E \end{cases} \quad (1)$$

where E, ε, σ, σ_y, and n are Young's modulus, strain, stress, yield stress, and the strain-hardening index, respectively. n is generally less than 0.5. The corresponding constitutive relation in three dimensions can be established using the von Mises flow rule [17] with strain hardening. The linear kinematic relations are used between the components of the strain tensor and the increments of the displacement field.

Without any body force, the mechanical equilibrium conditions are assumed valid during indentation,

$$\frac{\partial \sigma_{ij}}{\partial x_j} = 0 \quad (2)$$

where σ_{ij} ($i,j = 1, 2, 3$) are the components of the stress tensor, x_i are the components of the position vector of a material point.

As shown in Fig. 1, a rigid, spherical indenter is pressed onto the surface of a semi-infinite elastoplastic material. The contact boundary conditions in a cylindrical coordinate (r, θ, z) are

$$\sigma_{rz}(r,0) = 0 \quad \text{for } r < a \quad (3)$$

$$u_z(r,0) = f(r) - \delta \quad \text{for } r < a \quad (4)$$

where σ_{rz} and σ_{zz} are, respectively, the shear and normal components of the stress tensor, u_z is the displacement component along the loading direction, $f(r)$ is the surface profile of the indenter tip, δ is the displacement of the indenter, and a is the radius of the contact area to be determined in the simulation. Equation 3 represents the condition of frictionless contact between the indenter and the material. Outside the contact area, the surface is at stress-free state, i.e.

$$\sigma_{rz}(r,0) = \sigma_{zz}(r,0) = 0 \quad \text{for } r > a \quad (5)$$

The far field condition requires, $\sigma_{rz}(r,z) \to 0, \sigma_{zz}(r,z) \to 0, u_r(r,z) \to 0$, and $u_z(r,z) \to 0$ as $r \to \infty$ or $z \to -\infty$. The indentation load applied to the indenter can be calculated as

$$F = -2\pi \int_0^a \sigma_{zz}(r,0) r \mathrm{d}r \quad (6)$$

For $\sigma_y \to \infty$, the indentation problem reduces to the elastic contact between a rigid sphere and an elastic half-space. The closed-form solution is due to Hertz [1]. Sneddon [4] later derived a general load–displacement relation for elastic indentation of semi-infinite materials by a rigid, axisymmetric indenter, in which the contact between the indenter and the material is frictionless. For the contact radius being much less than the radius of the spherical indenter (i.e. the separation between the surface of the spherical indenter and the surface of an elastic halfspace is approximated as $r^2/2R$), the relations among the contact radius, the displacement of the spherical indenter, and the indentation depth are

$$a = \left(\frac{3(1-\nu^2)FR}{4E}\right)^{1/3} \quad \text{and} \quad \delta = \frac{a^2}{R} \quad (7)$$

where R is the radius of the spherical indenter, and ν is the Poisson ratio of the material.

Numerical simulation

As mentioned in previous section, it is impossible to obtain a closed-form solution for the indentation problems of elastoplastic materials. To study deep indentation of an elastoplastic material, the finite element method is used with focus on the effect of strain hardening. The simulation uses commercial finite element code of ABAQUS 6.6-1 (Dassault Systèms Simulia Corp. Providence, RI). The overall size of the finite element model is taken large enough to ensure the characteristic of a half space. The ratio of the radius of the rigid, spherical indenter to the length of the geometrical model is 1:12 along the loading and radial directions to allow for considerable decrease in deformation before reaching constrained boundaries. The nodes along the axisymmetric axis are constrained in the radial direction to simulate axisymmetric nature of the problem, and the nodes on the bottom side of the model are constrained in the z-direction. Generally, the indentation deformation can be divided into the loading and unloading of the indenter onto and out of the material. In the simulation, the loading and unloading are done in two steps by controlling the displacement of the indenter.

Figure 2 shows the finite element mesh used in the simulation. Fine mesh is used just adjacent to the indenter, and the element size gradually increases away from the indenter. The element CAX4R (axi-symmetrical element with four nodes and quadrilateral cross-section) is used. There are two degrees of freedom at each node, one in the radial direction and the other in the z-direction. The indenter is modeled as an analytically rigid surface. The contact formulation is applied between the analytically rigid indenter and the surface of the material. The frictionless contact is incorporated in the contact formulation of the indenter and the specimen.

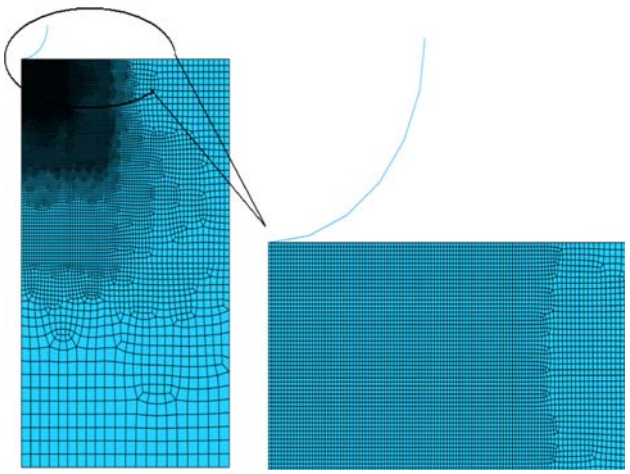

Fig. 2 Finite element model of the indentation deformation

Table 1 Material properties of AA6061-T6

Material	E (GPa)	Poisson ratio	Yield stress (MPa)
AA 6061-T6	69	0.33	255

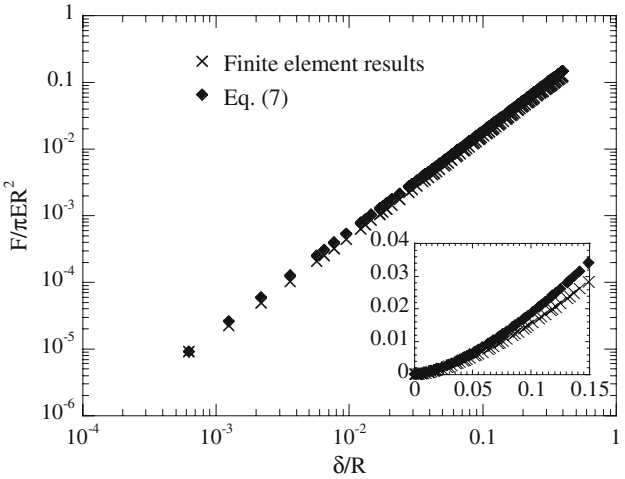

Fig. 3 Comparison of the finite element results with the Hertzian contact theory

In the simulation, the radius of the spherical indenter is 50 μm. Table 1 lists the material properties (elastic properties and yield stress).

To examine the validation of the finite element model, elastic indentation is performed first with frictionless contact between the indenter and the material. The solutions for the dependence of the indentation depth on the indentation load are compared to the Hertzian contact theory, as shown in Fig. 3. For $\delta/R \leq 1.25 \times 10^{-3}$, the finite element results are the same as those given by the Hertzian contact theory, while for $\delta/R > 1.25 \times 10^{-3}$ the finite element results deviate from the Hertzian contact theory. The percent error is 19% for $\delta/R > 0.01$. The Hertzian contact theory cannot accurately describe the deformation created by deep indentation, as expected.

Results and discussion

The finite element simulation has been performed by using the condition of frictionless contact between the indenter and the material. The indentation results are normalized by using the parameters of $F/\pi ER^2$ and δ/R for the indentation load and the indentation depth, respectively. Figure 4 shows the indentation loading–unloading curves for the strain-hardening indexes of 0, 0.1, 0.2, 0.3, and 0.4. Clearly, higher indentation load is required to make the same indentation depth for the materials of large strain-hardening index than that for the materials of small

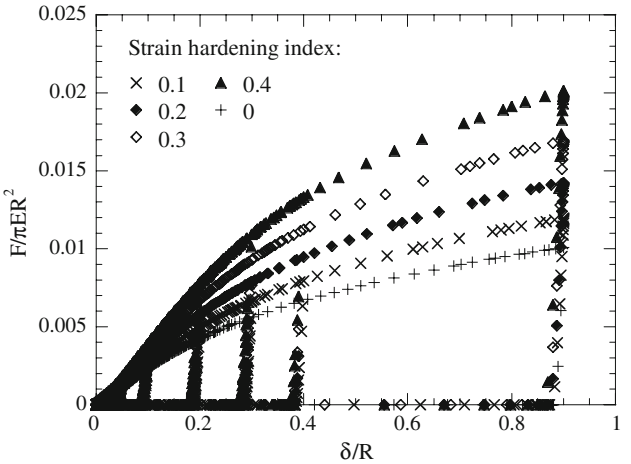

Fig. 4 Typical indentation loading–unloading curves for various strain-hardening indexes

strain-hardening index. The strain hardening has no significant effect on the slope of the unloading curves at the onset of the unloading, as expected. This suggests that the unloading behavior is controlled by the elastic properties of materials if there is no change in the microstructure and defects of materials. It is worth mentioning that there exist numerous dislocations and dislocation networks in metals, which could alter the unloading behavior of metals due to plastic recovery. However, this work only focuses on the indentation deformation from continuum plasticity.

Figure 5 shows the effect of the strain-hardening index on the ratio of the dimensionless force, $F/\pi ER^2$, to the dimensionless indentation depth, δ/R. In general, the ratio increases with the increase in the strain-hardening index for the same indentation depth due to the strain-hardening behavior. However, approximately linear relation between the strain-hardening index and the ratio is observed for $\delta/R < 0.05$ and $\delta/R \geq 0.2$. The ratio reaches the maximum value at $\delta/R \approx 0.1$, dependent of the strain-hardening index. Such a behavior reveals the effect of the indenter size on the indentation deformation. The indentation deformation is a complicated function of the strain-hardening index and the indentation load, even though the indentation depth increases with the increase in the indentation load.

In general, the indentation load is a power function of the indentation depth with the power in the range of 1.2–2 for shallow indentation. Figure 6 shows the dependence of the ratio on the indentation depth for different strain-hardening indexes. The ratio increases first with increasing the indentation depth, reaches the maximum value, and then decreases with the indentation depth. The results suggest that the relation between the indentation depth and the indentation load cannot be simply described by a power function. Actually, such a power law relation can only hold

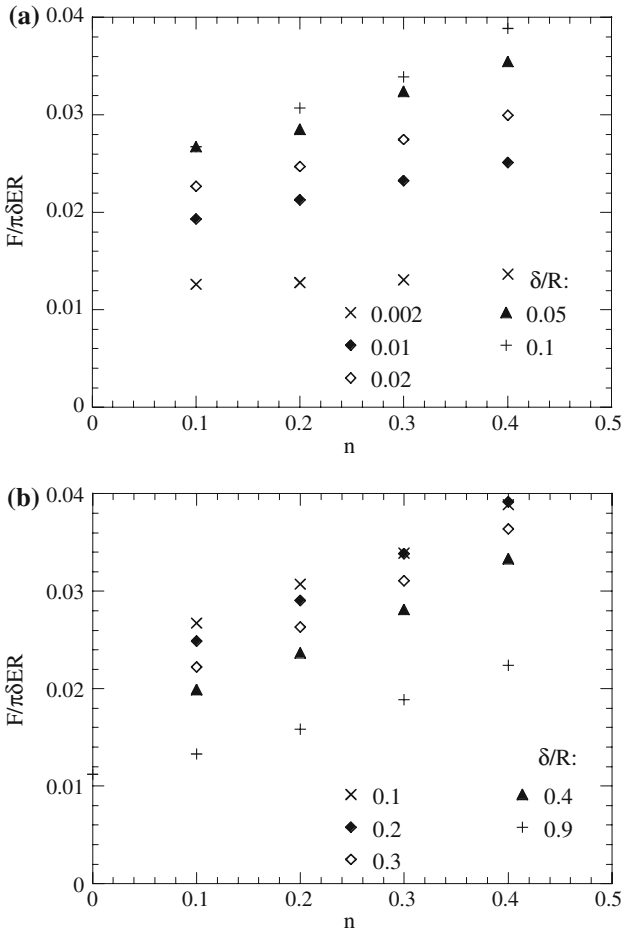

Fig. 5 Dependence of the ratio of the dimensionless load ($F/\pi ER^2$) to the dimensionless depth (δ/R) on the strain-hardening index; (**a**) the results for $\delta/R \leq 0.1$ and (**b**) the results for $\delta/R \geq 0.1$

for shallow indentation of $\delta/R \leq 0.05$ for $0.1 \leq n \leq 0.4$, as shown in Fig. 6. Caution needs to be taken in analyzing experimental results for indentations by rigid, spherical indenters.

From the computed indentation loading–unloading curve, one can calculate the total mechanical work done to the material as

$$W = \int_0^{\delta_{\max}} F \mathrm{d}\delta \tag{8}$$

where $\delta_{\max}$ is the maximum indentation depth. The mechanical work can be calculated from the area under the indentation loading curve. One can calculate the elastic recovery energy released during the unloading process, E_{elastic}, as

$$E_{\text{elastic}} = \int_{\delta_r}^{\delta_{\max}} F_{un} \mathrm{d}\delta \tag{9}$$

where δ_r is the residual indentation depth. The elastic recovery energy can be evaluated from the area under the

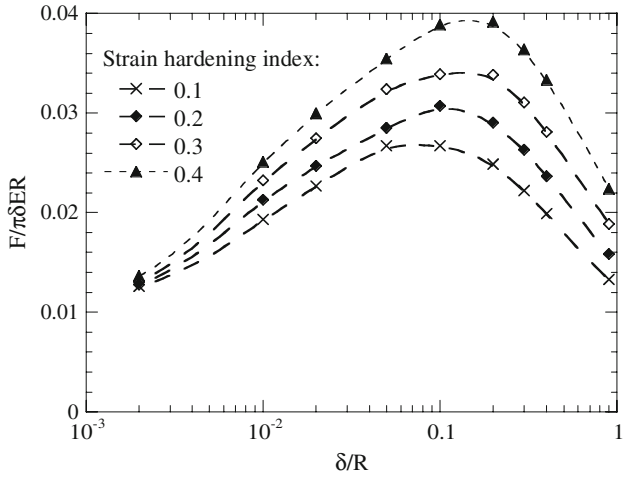

Fig. 6 Dependence of the ratio of the dimensionless load ($F/\pi ER^2$) to the dimensionless depth (δ/R) on the indentation depth for different strain-hardening indexes

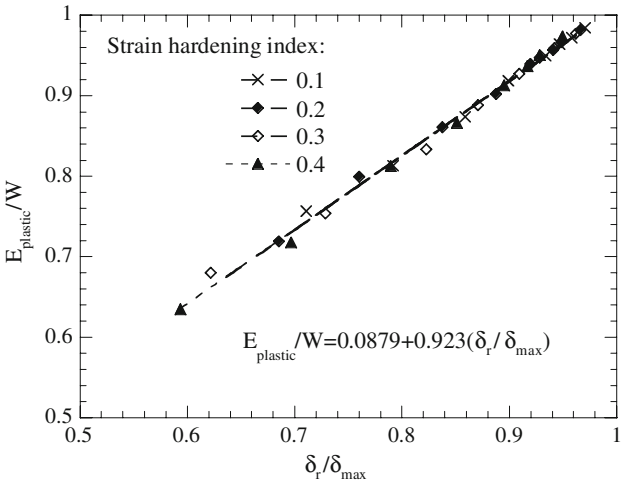

Fig. 7 Dependence of the energy ratio, E_{plastic}/W, on the depth ratio, $\delta_r/\delta_{\max}$ for various strain-hardening indexes

unloading curve. Thus the plastic energy dissipated in an indentation loading–unloading cycle, E_{plastic}, as represented by the area enclosed by the indentation loading–unloading curve and the depth axis, is given as

$$E_{\text{plastic}} = W - E_{\text{elastic}} \tag{10}$$

It has been proposed [18] for sharp indenters that there exists a linear relationship between the energy ratio, E_{plastic}/W, and the indentation depth ratio, $\delta_r/\delta_{\max}$, for $\delta_r/\delta_{\max} > 0.4$. Figure 7 shows the dependence of the energy ratio on the indentation-depth ratio for the indentation depth up to $0.9R$. Clearly, the energy ratio is a linear function of the indentation-depth ratio in accordance with the results for indentation by sharp indenters [18]. Using curve-fitting for a linear function, the relation between the energy ratio and the indentation-depth ratio can be written as

$$\frac{E_{\text{plastic}}}{W} = 0.0879 + 0.923\frac{\delta_r}{\delta_{\max}} \tag{11}$$

one can obtain the extrapolated value of the energy ratio as $\delta_r/\delta_{\max} \to 0$. The extrapolated value of the energy ratio is 0.0879 in contrast to the value of -0.27 given by Cheng et al. [18] for sharp instrumented indentations. Such a difference is likely due to the shape effect of the indenter tip, which creates different stress field underneath the indenter and different plastic deformation zone. Severer plastic deformation is made by sharp indenters than those by spherical indenters. As shown in Fig. 7, there are always slight deviations from the linear relation of (11) for different strain-hardening indexes, suggesting that Eq. 11 can only describe the general trend between the energy ratio and the indentation depth ratio. For each specific material, the exact relation between the energy ratio and the indentation depth ratio will be slight different. This could be the reason that Eq. 11 is different from the relationship proposed by Ni et al. [16] for the spherical indentation of elastoplasic materials with the mechanical properties of $\sigma_y/E = 0.025$, $v = 0.2$, and $n = 0.5$, even though the linear relation could be regarded as "universal". It is worth mentioning that it is unclear if the linear relation is valid for the materials with gradient of strain hardening along the loading direction.

One of important parameters affecting the analysis of the indentation deformation is the size of the pile-up. Figure 8 shows the dependence of the pile-up on the strain-hardening index at the maximum indentation depth of $0.9R$. The pile-up linearly decreases with the increase in the strain-hardening index. The material has larger pile-up at the unloading state than that subjected to the peak indentation load. During the unloading, elastic recovery occurs which allows material to move to the self-equilibrium state.

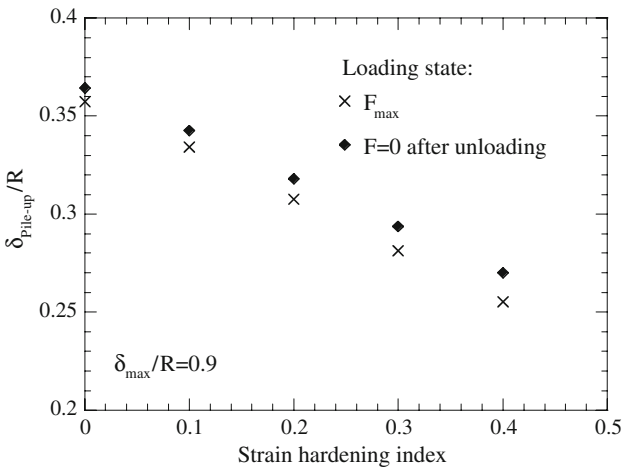

Fig. 8 Dependence of the pile-up on the strain-hardening index

Summary

The finite element analysis has been used to simulate the deep indentation of strain-hardening, elastoplastic materials by a rigid, spherical indenter. The displacement of the indenter has been pushed up to 90% of the radius of the spherical indenter onto the materials. A linear relation is observed between the strain-hardening index and the ratio of the peak indentation load to the maximum indentation depth. The power law relation between the indentation load and the indentation depth is only valid for shallow indentation of the maximum indentation depth up to 5% of the indenter radius. For deep indentation, the power law relation breaks, and caution needs to be taken in analyzing experimental results for deep indentations by spherical indenters. Similar to sharp instrumented indentation for the ratio of the residual indentation depth to the maximum indentation depth larger than 0.57, the ratio of the plastic energy to the total mechanical work is a linear function of the ratio of the residual indentation depth to the maximum indentation depth for the indentations by spherical indenters, independent of the strain-hardening index. However, the extrapolated value of the energy ratio is different from that for the sharp instrumented indentation.

Acknowledgement This work is supported by National Science Foundation through the grant CMS-0508989 and Kentucky Science and Engineering Foundation.

References

1. Hertz H (1882) J Reine Angew Math 92:156
2. Love AEH (1939) Q J Math 10:161. doi:10.1093/qmath/os-10.1.161
3. Love AEH (1944) A treatise on the mathematical theory of elasticity, 4th edn. Dover, New York
4. Harding JW, Sneddon IN (1945) Proc Camb Philos Soc 41:16
5. Mindlin RD, Deresiewicz H (1953) J Appl Mech Trans ASME 20:327
6. Yang FQ (2003) Mater Sci Eng A 358:226. doi:10.1016/S0921-5093(03)00289-2
7. Yang FQ (1998) Mech Mater 30:275. doi:10.1016/S0167-6636(98)00035-0
8. Shih CW, Yang M, Li JCM (1991) J Mater Res 6:2623. doi:10.1557/JMR.1991.2623
9. Montmitonnet P, Edlinger ML, Felder E (1993) J Tribol Trans ASME 115:10. doi:10.1115/1.2920962
10. Sadeghipour K, Chen W, Baran G (1994) J Phys D Appl Phys 27:1300. doi:10.1088/0022-3727/27/6/030
11. Shu JY, Fleck NA (1998) Int J Solids Struct 35:1363. doi:10.1016/S0020-7683(97)00112-1
12. Taljat B, Zacharia T, Kosel F (1998) Int J Solids Struct 35:4411. doi:10.1016/S0020-7683(97)00249-7
13. Yang FQ (1998) Int J Mech Sci 40:87. doi:10.1016/S0020-7403(97)00035-0
14. Yang FQ, Li JCM (1995) Mater Sci Eng A 201:50. doi:10.1016/0921-5093(95)09763-5
15. Yang FQ, Saran A (2006) J Mater Sci Lett 41:6077
16. Ni WY, Chen YT, Cheng CM, Grummon DS (2004) J Mater Res 19:149. doi:10.1557/jmr.2004.19.1.149
17. Dieter GE (1988) Mechanical metallurgy. McGraw Hill, New York
18. Cheng YT, Li ZY, Cheng CM (2002) Philos Mag A 82:1821